Ligand Effects on Hydrogen Atom Transfer from Hydrocarbons to Three-Coordinate Iron Imides

Ryan E. Cowley and Patrick L. Holland*

Department of Chemistry, University of Rochester, Rochester, New York 14627, United States

Ⓢ *Supporting Information*

ABSTRACT: A new β-diketiminate ligand with 2,4,6-tri-(phenyl)phenyl *N*-substituents provides protective bulk around the metal without exposing any weak C−H bonds. This ligand improves the stability of reactive iron(III) imido complexes with Fe═NAd and Fe═NMes functional groups (Ad = 1-adamantyl; Mes = mesityl). The new ligand gives iron(III) imido complexes that are significantly more reactive toward 1,4-cyclohexadiene than the previously reported 2,6-diisopropylphenyl diketiminate variants. Analysis of X-ray crystal structures implicates Fe═N−C bending, a longer Fe═N bond, and greater access to the metal as potential reasons for the increase in C−H bond activation rates.
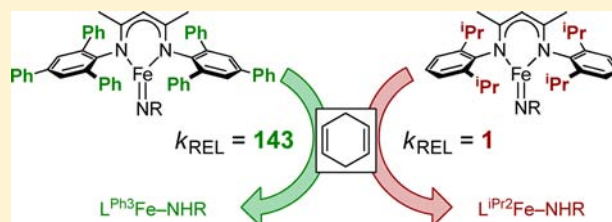
INTRODUCTION

Hydrogen atom transfer (HAT) is an elementary reaction in which both a proton and an electron are moved in a single kinetic step.[1] Many metal−oxo (M═O) complexes are known to abstract H-atoms from organic substrates to form metal−hydroxo complexes,[2] both in biological[3] and model systems.[4] The imido ligand is isoelectronic to the oxo ligand, but HAT is less well studied for metal−imido (M═NR) complexes. HAT reactions to imido ligands are rarely observed directly,[5] despite the strong implication of HAT in many systems.[6] For imidometal complexes, the N substituent enables electronic and steric tuning of the imido fragment, a feature not available in oxo complexes. Therefore, comparing HAT rates for metal−imido complexes containing different imido *N*-substituents can help elucidate electronic and steric effects on the HAT mechanism.

Previously, the (β-diketiminato)iron imido complex $L^{Me,iPr2}$FeNAd ($L^{Me,iPr2}$ = 2,4-bis(2,6-diisopropylphenylimido)-3-pentyl; Ad = 1-adamantyl) was reported,[7] and it was capable of abstracting hydrogen atoms from 1,4-cyclohexadiene (CHD) and other related hydrocarbons in the presence of 4-*tert*-butylpyridine (^{t}Bupy).[8−10] In the absence of substrate, the imido complex decayed by intramolecular HAT by abstracting H• from one of the flanking isopropyl groups of the β-diketiminate ligand. This intramolecular decomposition limited the imido complex to activating C−H bonds that were significantly weaker than the benzylic C−H bonds of the isopropyl groups (ca. 84 kcal/mol). As part of our efforts to design systems that prevent unwanted attack on the supporting ligand, we report here a modified ligand $L^{Me,Ph3}$ ($L^{Me,Ph3}$ = 2,4-bis(2,4,6-triphenylphenylimido)-3-pentyl) that features phenyl groups in place of isopropyl substituents,[11] and which places no weak C−H bonds near the metal center. Using this new ligand, we have prepared the new iron(III) imido complexes

$L^{Me,Ph3}$FeNAd and $L^{Me,Ph3}$FeNMes, which are more stable in the absence of substrate than $L^{Me,iPr2}$FeNAd, and have found that their HAT rate constants correlate with imido ligand basicity. Finally, we show that the HAT rate is modulated by the supporting β-diketiminate ligand, and that the shape of the binding pocket is more important than simple measures of ligand size for rationalizing HAT reactivity.

RESULTS AND DISCUSSION

Preparation of a Novel Diketiminate and its Iron(II) Complex. The most common synthetic route to the diketimine proligand is the acid-catalyzed condensation between a diketone and 2 equiv of an amine.[12] Following this precedent, heating 2 equiv of 2,4,6-triphenylaniline with 2,4-pentanedione in the presence of 1 equiv of HOTs (Ts = *p*-tolylsulfonyl) affords the novel diketimine $L^{Me,Ph3}$H (**1**) (Scheme 1). The rate of this condensation reaction is much slower than similar condensation reactions with bulky anilines such as 2,6-diisopropylaniline. In the reaction to form **1**, refluxing in toluene (bp 111 °C) afforded only ∼70% conversion after 10 days; however, full conversion can be achieved in refluxing xylenes (bp 139−141 °C) within 24 h. Ligand **1** was isolated as a bright yellow crystalline solid in 74% yield after basic workup and crystallization from CH_2Cl_2/MeOH. Extended heating under vacuum (120 °C for 12 h) was required to completely remove solvent trapped in the solid.

The crystal structure of **1** (Figure 1) reveals that **1** exists in the solid state as the enaminoimine tautomer. The downfield N−H resonance in the ^{1}H NMR spectrum at δ 12.2 ppm is consistent with the enamine proton that is engaged in an intramolecular hydrogen bond, and suggests that the

Scheme 1. Synthesis of the Ligand $L^{Me,Ph3}H$ (1) and Its Li (2) and FeBr (3) Complexes[a]
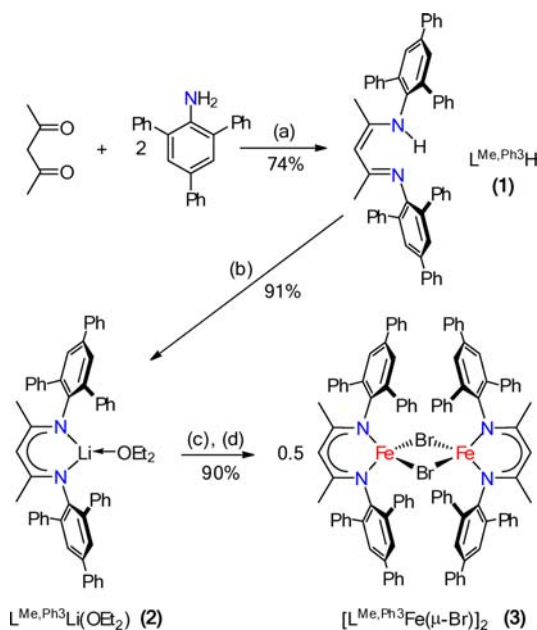
[a]Reagents and conditions: (a) TsOH·H$_2$O, 24 h, reflux with Dean−Stark condenser, xylenes. (b) ^{n}BuLi, 4 h, Et$_2$O/hexanes. (c) FeBr$_2$, 14 h, THF, 25 °C. (d) toluene, 100 °C.

Figure 1. Molecular structure of $L^{Me,Ph3}H$ (1) with thermal ellipsoids shown at 50% probability. Hydrogen atoms except the amine hydrogen are removed for clarity. Relevant bond distances (Å): N11−C21 1.309(2); C21−C31 1.423(2); C31−C41 1.384(2); C41−N21 1.341(2).

enaminoimine is the only tautomer present at room temperature.

Deprotonation of **1** with ^{n}BuLi in Et$_2$O produces the bright yellow complex $L^{Me,Ph3}Li(OEt_2)$ (**2**). The ^{1}H NMR spectrum of **2** shows upfield-shifted resonances for the diethyl ether hydrogens (δ 2.68, 0.27 ppm) consistent with coordination to the Li^{+} ion. Integration of the OEt$_2$ resonances indicates a 1:1 ligand/OEt$_2$ ratio, consistent with a single coordinated OEt$_2$ ligand. X-ray crystallography of Li complexes with other β-diketiminate ligands has revealed similar etherate stoichiometry, for example in the trigonal complexes $L^{Me,iPr2}Li(OEt_2)$,[13] $L^{tBu,iPr2}Li(THF)$,[14] and $L^{Me,F6}Li(OEt_2)$.[15] The structure of **2** as a trigonal mono(ether) complex is thus likely to be similar. In solution, complex **2** emits an intense cyan fluorescence (emission λ_{max} = 475 nm, see Figure 2), presumably from a $\pi \rightarrow \pi^{*}$ transition involving the conjugated orbitals. The protonated ligand **1** is also bright yellow in color, but does
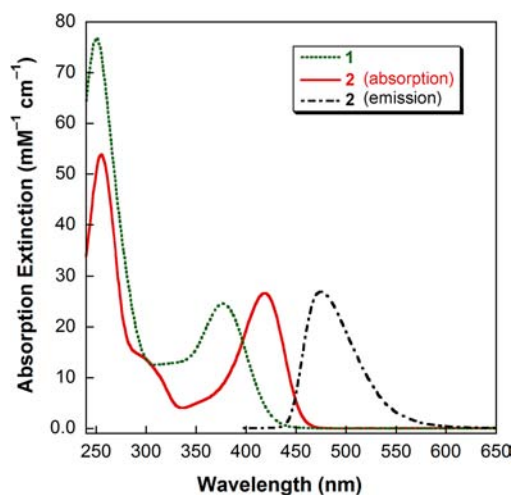
Figure 2. Absorption spectra for $L^{Me,Ph3}H$ (**1**) in CH$_2$Cl$_2$ and $L^{Me,Ph3}Li(OEt_2)$ (**2**) in Et$_2$O, and normalized emission spectrum of **2** in Et$_2$O with excitation wavelength λ_{ex} = 395 nm.

not fluoresce when excited near its maximum absorption at 377 nm.

The orange-red iron(II) bromide complex of the $L^{Me,Ph3}$ ligand was prepared in 90% yield from **2** and FeBr$_2$ in THF (Scheme 1). The identity of the complex as the dimer $[L^{Me,Ph3}Fe(\mu\text{-}Br)]_2$ (**3**) was revealed by X-ray crystallography, and the molecular structure of **3** is shown in Figure 3. Each iron center is coordinated by a diketiminate ligand and two bridging bromides in a pseudotetrahedral geometry.
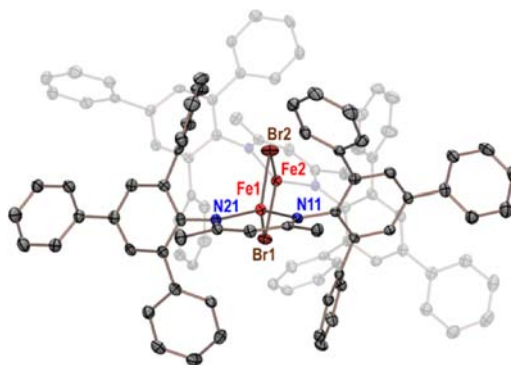
Figure 3. Molecular structure of $[L^{Me,Ph3}Fe(\mu\text{-}Br)]_2$ (**3**) with thermal ellipsoids shown at 50% probability. Cocrystallized solvent molecules and hydrogen atoms are removed, and the back half of the dimer is shown in light gray for clarity. Relevant bond distances (Å) and angles (deg): Fe1−Br1 2.5311(7); Fe1−Br2 2.5050(6); Fe2−Br1 2.5420(6); Fe2−Br2 2.5500(7); Fe1−N11 2.017(3); Fe1−N21 2.007(3); Fe1−Br1−Fe2 93.05(2); Fe1−Br2−Fe2 93.48(2).

The planes defined by the diketiminate backbones are twisted 33.9(1)° with respect to each other. This twist also rotates the N-aryl groups on adjacent ligands to accommodate their flanking *ortho* phenyl substituents. In solution, however, the molecule displays apparent D_{2d} symmetry as evidenced by the 11 resonances in the ^{1}H NMR spectrum, which implies that the aryl substituents on opposite sides of the dimer are able to move past each other in solution. In THF-d_8 solution, the color of **3** changes from orange-red to yellow, suggesting the formation of monomeric $L^{Me,Ph3}Fe(Br)(THF)$, analogous to

other yellow solvento species such as $L^{Me,iPr2}Fe(Br)(THF)$,[16] $L^{tBu,iPr2}Fe(Cl)(NCMe)$,[17] and $L^{tBu,iPr2}Fe(Cl)(3\text{-picoline})$.[18]

Reduction of Iron(II) Affords an Iron(I) Arene Complex. When performed under an N_2 atmosphere, single-electron reduction of other iron(II) diketiminate complexes in ethereal solvents gives either the corresponding high-spin diiron dinitrogen complexes $L^{R,R'}Fe(\mu\text{-}N_2)FeL^{R,R'}$,[19] or an iron-nitride as the result of N_2 cleavage.[20] However, addition of 2 equiv of KC_8 to a slurry of **3** under N_2 affords a product (**4**) that does not incorporate N_2 (Scheme 2).

Scheme 2. Reduction of 3 to Afford the Iron(I) Monomer 4
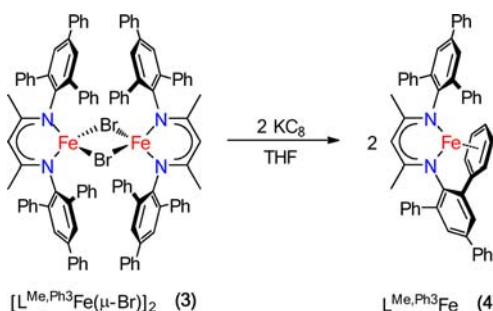
The structure of **4** was revealed by X-ray crystallography, and its molecular structure is shown in Figure 4. One of the *ortho*
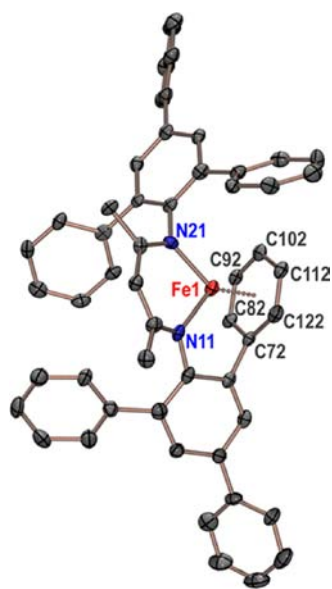
Figure 4. Molecular structure of $L^{Me,Ph3}Fe$ (**4**) with thermal ellipsoids shown at 50% probability. Cocrystallized solvent molecules and hydrogen atoms are removed for clarity. Relevant bond distances (Å) and angles (deg): Fe1−N11 1.936(5); Fe1−N21 1.960(5); Fe1−C72 2.034(5); Fe1−C82 2.076(6); Fe1−C92 2.128(6); Fe1−C102 2.138(6); Fe1−C112 2.160(6); Fe1−C122 2.098(6); N11−Fe1−N21 93.6(2); Fe1−C$_{centroid}$ 1.564(6); N11−Fe1−C$_{centroid}$ 125.7(4); N21−Fe1−C$_{centroid}$ 140.7(4).

phenyl rings coordinates to the iron center in an η^6 fashion, which requires significant *N*-aryl rotation and bending at the *ipso* carbon. Interestingly, toluene solvent molecules pack into the crystal lattice of **4** in a 2:1 toluene/Fe ratio; however, the complex lacks any Fe···toluene interactions. This demonstrates that an intramolecular arene contact is favored over

intermolecular contacts, at least in the solid state (the possibility of binding exogenous arenes in solution is addressed below). There are other examples of diketiminate arene moieties coordinating to metal(I) complexes, in the mono-nuclear complex $L^{tBu,iPr2}Co$,[21] and in the dimers $[L^{Me,Me2}Cu]_2$,[22] $[L^{Me,R2}Ni]_2$ (R = Et, ^iPr),[23] and $[L^{Me,R2}V]_2$ (R = Et, ^iPr),[24] but the structure of **4** with *N,N'* coordination and an intramolecular metal−(η^6-arene) association is unique among mononuclear diketiminate complexes.

The ^1H NMR spectrum of **4** has no observable resonances, which is reminiscent of other low-spin ($S = ^1/_2$) iron(I) complexes such as $L^{R,iPr2}Fe(CN^tBu)_{2,3}$ (R = Me, ^tBu)[25,26] and $L^{R,iPr2}Fe(CO)_{2,3}$ (R = Me, ^tBu).[19b,27] The $S = ^1/_2$ spin state of **4** was also established from electron paramagnetic resonance (EPR) spectroscopy: a spectrum of **4** recorded at 50 K in a frozen 2-methyltetrahydrofuran (2-MeTHF) solution showed a single rhombic signal with **g** = [2.186, 2.012, 1.979] (Figure 5)
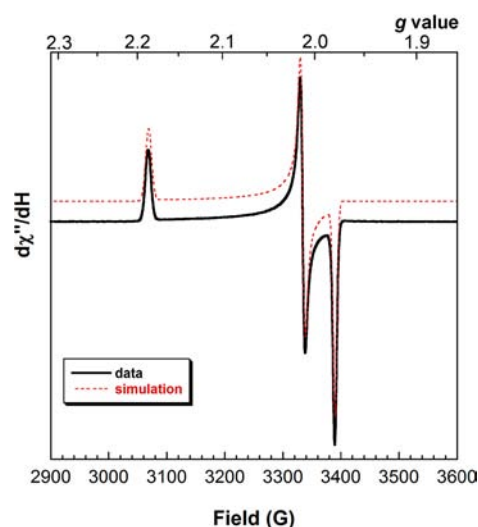
Figure 5. X-band EPR spectrum of $L^{Me,Ph3}Fe$ (**4**) in frozen 2-methyltetrahydrofuran solution recorded at 50 K. Acquisition parameters: frequency = 9.3891 GHz, power = 0.1 mW, conv. time = 35 ms, mod. amplitude = 0.7 G, mod. frequency = 30 kHz, time const. = 41 ms. The dashed line represents a $S = ^1/_2$ simulation with **g** = [2.186, 2.012, 1.979].

that resembles the spectrum of the previously characterized iron(I)-benzene complex $L^{Me,iPr2}Fe(\eta^6\text{-}C_6H_6)$ (**g** = [2.20, 2.01, 1.98]).[19b] The solution magnetic moment (μ_{eff} = 1.8(1) BM) measured by the Evans method in C_6D_{12} suggests that the low-spin monomer formulation is maintained in solution. To test whether toluene can displace the intramolecular arene arm in solution, the EPR spectrum of **4** was recorded in neat toluene. The EPR spectra in toluene and 2-MeTHF were identical (maximum deviation in $g < 0.001$), suggesting that the structure is identical in each solvent, and an intermolecular Fe-arene interaction is disfavored. This is in concord with the crystallographic observation of noninteracting toluene molecules, described above.

Synthesis of Iron-Imido Complexes. The most convenient method for the preparation of a M^{n+} imido complex is through nitrene capture from an organoazide by a reduced $M^{(n-2)+}$ precursor, and thus we endeavored to use **4** as a source of Fe(I) in the synthesis of Fe(III) imides. Addition of N_3Ad (Ad = 1-adamantyl) or N_3Mes (Mes = mesityl; 2,4,6-trimethylphenyl) to a solution of the iron(I) synthon **4**

(Scheme 3) results in effervescence and the appearance of new paramagnetically shifted ^{1}H NMR resonances and EPR signals

Scheme 3. Synthesis of Imido Complexes L^{Me,Ph3}FeNAd (5) and L^{Me,Ph3}FeNMes (6)
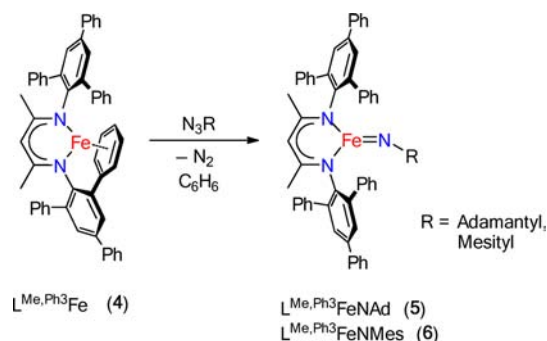
consistent with formation of intermediate-spin iron(III) imido products L^{Me,Ph3}FeNAd (**5**) and L^{Me,Ph3}FeNMes (**6**). Significantly, the imido products featuring the L^{Me,Ph3} ligand are much more stable in solution than their previously reported analogues supported by the L^{Me,iPr2} ligand.[8,9,26] Complexes **5** and **6** may be handled in C$_6$D$_6$ for several days at ambient temperature without significant decomposition, which contrasts to the relatively low stability of L^{Me,iPr2}FeNAd and of L^{tBu,iPr2}FeNAd (solution lifetimes ~1 d) and apparent instability of L^{Me,iPr2}FeNMes (attempts at synthesis resulted in immediate decomposition).

In the ^{1}H NMR spectrum of the crude product of the reaction of **4** with N$_3$Ad, several resonances appear at chemical shifts that are very similar to those in the three-coordinate imido complex L^{Me,iPr2}FeNAd, which initially suggested that the products have a similar geometry and electronic structure. Crystallization from pentane at −45 °C afforded plate-like crystals suitable for X-ray diffraction, and the structure of the product L^{Me,Ph3}FeNAd (**5**) is shown in Figure 6. Like
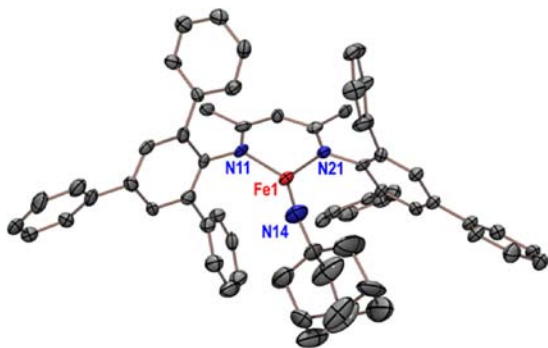
Figure 6. Molecular structure of L^{Me,Ph3}FeNAd (**5**) shown with 50% probability thermal ellipsoids. Hydrogen atoms are removed for clarity. Relevant bond distances (Å) and angles (deg): Fe1−N14 1.700(5); Fe1−N11 1.961(4); Fe1−N21 1.962(4); Fe1−N14−C14 151.2(5); N11−Fe1−N14 139.0(2); N21−Fe1−N14 126.7(2).

L^{Me,iPr2}FeNAd,[7] complex **5** features a planar three-coordinate iron center, in which the sum of angles at iron is 360.1(3)°. Compared to L^{Me,iPr2}FeNAd, compound **5** has a longer Fe≡N bond (1.700(5) versus 1.670(2) Å), and a more bent Fe≡N−C angle (151.2(5) versus 170.4(2)°). These structural features may explain the greater reactivity of **5** (see below), but it is

important to note that the crystallographic fit gives an imido N atom with a large thermal ellipsoid, and there is accordingly significant uncertainty in the position of this atom that may not be fully captured in the estimated standard deviation.

The arylimido complex L^{Me,Ph3}FeNMes (**6**) was synthesized from **4** and N$_3$Mes in an analogous manner to the synthesis of **5**. Although **6** did not afford crystals of sufficient quality for X-ray structure determination, the X-band EPR spectra of **5** and **6** are similar (Figure 7), suggesting a similar geometric structure.
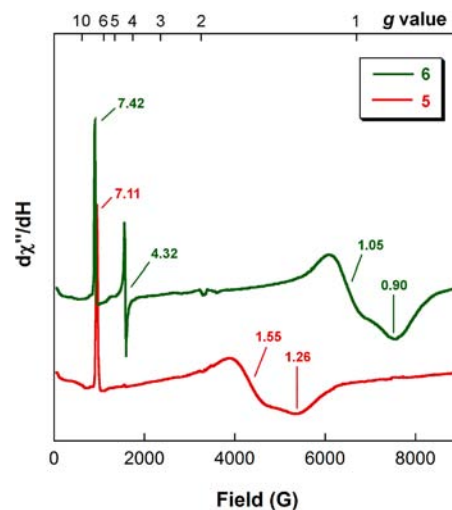
Figure 7. X-band EPR spectra of imido complexes **5** and **6** recorded in frozen toluene solution at 8 K. Acquisition parameters: frequency = 9.39 GHz, power = 0.1 mW, conv. time = 35 ms, mod. amplitude = 6.1 G, mod. frequency = 30 kHz, time const. = 66 ms. The g_{eff} value for each spectral feature is indicated.

Both **5** (g_{eff} = 7.11, 1.55, 1.26) and **6** (g_{eff} = 7.42, 1.05, 0.90) show rhombic EPR signals characteristic of $S = \frac{3}{2}$ paramagnets, and these are similar to the spectra of the imido complexes L^{Me,iPr2}FeNAd and L^{tBu,iPr2}FeNAd (Supporting Information, Table S-2 and Figure S-3).[7,26] In the EPR spectrum of **5**, an additional isotropic feature at g_{eff} = 4.32 is evident, which is attributed to a small amount of an $S = \frac{5}{2}$ impurity. Double integration of the spectrum suggests that this impurity accounts for <0.5% of the total signal (Supporting Information, Figure S-4).

It is interesting to compare this synthetic method to the one used earlier from dinuclear L^{Me,iPr2} and L^{tBu,iPr2} supported dinitrogen complexes.[7,8,26] The successful preparation of monomeric iron(III) imido complexes from the earlier N$_2$ complexes required the use of a coordinating solvent or pyridine additive; otherwise the azide was reductively coupled to give a dinuclear hexaazadienyldiiron(II) product with six catenated nitrogen atoms.[28] We have proposed that azide coupling results from the preorganization of iron centers by the LFeNNFeL starting material, whereas the addition of a donor solvent led to monoiron species that prefer to eliminate N$_2$ in an intramolecular reaction.[7] In this context, notice that *monomeric* L^{Me,Ph3}Fe (**4**) reacts with azides in a poor donor solvent to give only imido products, without azide coupling. This observation fits the proposed model,[7] and suggests that the hemilabile L^{Me,Ph3} ligand plays a useful role in modulating the reactivity of the iron(I) synthon.

H-Atom Abstraction Reactions. We have described details on the ability of L^{Me,iPr2}-supported iron(III) imido

complexes to activate the weak C−H bonds (~77 kcal/mol) of cyclohexadiene (CHD).[9] $L^{Me,Ph3}$FeNAd (**5**) reacts with excess (10 equiv) of CHD at room temperature, giving a 92% yield of the iron(II) amido product $L^{Me,Ph3}$FeNHAd (**5·H**) within 2 min, as judged by ^{1}H NMR spectroscopy. $L^{Me,Ph3}$FeNMes (**6**) reacts with CHD more sluggishly: 90% yield of the amidoiron product $L^{Me,Ph3}$FeNHMes (**6·H**) was achieved only after 12 h. Both amido complexes **5·H** and **6·H** can be prepared independently by anion metathesis from $[L^{Me,Ph3}Fe(\mu\text{-}Br)]_2$ (**3**), and the solid state structure of **6·H** is shown in Figure 8.
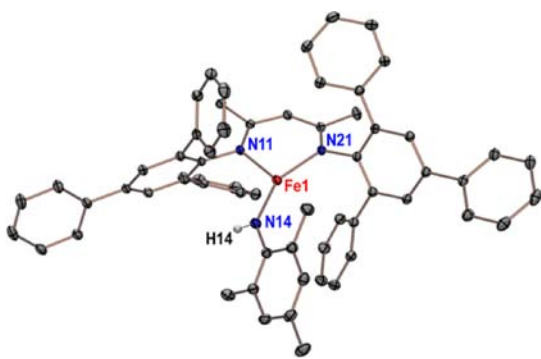
Figure 8. Molecular structure of $L^{Me,Ph3}$FeNHMes (**6·H**) with thermal ellipsoids shown at 50% probability. Hydrogen atoms except H14 are removed for clarity. Relevant bond distances (Å) and angles (deg): Fe1−N14 1.902(1); Fe1−N11 2.0112(9); Fe1−N21 1.9819(9); Fe1−N14−C14 139.35(8); N11−Fe1−N14 115.00(4); N21−Fe1−N14 150.62(4).

In the structure of **6·H**, the mesitylamido ligand is rotated by 52.8° relative to the diketiminate plane, presumably to relieve steric pressure between the mesityl and flanking *ortho*-phenyl groups. Complexes with less bulky anilido ligands such as $L^{tBu,iPr2}$FeNHPh feature coplanar anilido and diketiminate ligands (0.8° between planes),[29] supporting the notion that the NHMes rotation in **6·H** is sterically enforced in the solid state. The ^{1}H NMR spectrum of **6·H** shows only three resonances assigned to the mesityl group (with integrations 2:3:6), consistent with rapid mesityl rotation in solution.

The kinetics of the HAT reactions of **5** and **6** with CHD were monitored by ^{1}H NMR spectroscopy. Under pseudo-first-order conditions (excess CHD) at 10 °C, the observed rates of HAT (k_{obs}) showed a linear dependence on [CHD] (Supporting Information, Figures S-1 and S-2), implying the rate laws in eqs 1 and 2, where the factors of two account for the 2 equiv of H[•] that are supplied by each CHD molecule.[30]

$$-\frac{d[\mathbf{5}]}{dt} = 2k_5[\mathbf{5}][CHD] \tag{1}$$

$$-\frac{d[\mathbf{6}]}{dt} = 2k_6[\mathbf{6}][CHD] \tag{2}$$

The second-order rate constants for HAT are calculated from the slopes of Supporting Information, Figures S-1 and S-2 to be $k_5 = 2.0(2) \times 10^{-2}$ M^{-1} s^{-1} and $k_6 = 8.2(5) \times 10^{-5}$ M^{-1} s^{-1} at 10 °C (Table 1). Why is the HAT rate constant for **5** more than 2 orders of magnitude (240 ± 30 times) larger than the HAT rate constant for **6**? One hypothesis is that the more electron-donating adamantyl group in **5** increases the basicity of the imido ligand in **5** relative to **6**. To evaluate this hypothesis, the thermodynamics of HAT can be broken into proton

Table 1. Second-Order Rate Constants for HAT to Iron(III) Imido Complexes from 1,4-Cyclohexadiene in C_6D_6 Solution

complex	k_{HAT} at 10 °C (M^{-1} s^{-1})	$k_{rel}{}^a$
$L^{Me,iPr2}$Fe(NAd)(^{t}Bupy)	$4.4(3) \times 10^{-1}$	5400
$L^{Me,Ph3}$FeNAd (**5**)	$2.0(2) \times 10^{-2}$	240
$L^{Me,iPr2}$FeNAd	$1.4(2) \times 10^{-4}$	1.7
$L^{Me,Ph3}$FeNMes (**6**)	$8.2(5) \times 10^{-5}$	1
$L^{tBu,iPr2}$FeNAd	0^b	0^b

^{a}Relative to the rate constant for $L^{Me,Ph3}$FeNMes. ^{b}The complex $L^{tBu,iPr2}$FeNAd has not been observed to react with CHD, even with excess CHD at 25 °C. See ref 26.

transfer (PT) and electron transfer (ET) contributions in a thermodynamically constrained square (Figure 9), and more favorable PT or ET will result in more favorable HAT.
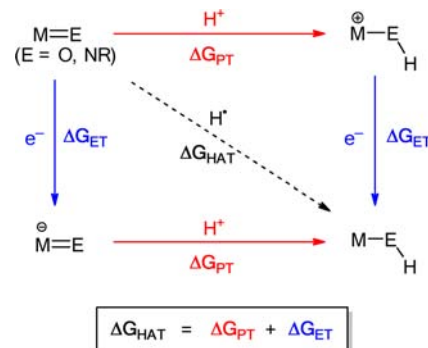
Figure 9. Thermodynamic square relating proton transfer (PT) and electron transfer (ET) to overall HAT free energy.

Previous studies have established that strongly basic imido and oxo ligands increase the thermodynamic driving force and rate of HAT by making proton transfer more exergonic. For example, heme enzymes utilize basic *trans* ligands to increase the reactivity of Fe=O intermediates toward HAT.[31] This trend has also been observed in synthetic iron and manganese oxo complexes, where more basic ligands *trans* to the oxo correlate with faster HAT rates.[32,33] In iron-imido chemistry, the addition of pyridine donors to $L^{Me,iPr2}$FeNAd increased the HAT rate by several orders of magnitude, and pyridines with electron-donating substituents led to even larger HAT rate constants, suggesting that pyridine modulated both the basicity and the reactivity of the imide toward HAT. A related effect may be responsible for the increased reactivity of **5** relative to **6**: the electron-donating adamantyl substituent in **5** renders the imido ligand more electron-rich, making ΔG for the PT contribution more favorable. Although increased imido basicity makes PT more favorable, ET will concomitantly become *less favorable*, since a more electron-rich metal is harder to reduce. Since the combined thermodynamic effect observed is that HAT is more favorable, *the free energy gain for the contribution from PT must outweigh the free energy penalty for making ET more difficult.* Finally, we note that the N−H bond in the alkylamido product **5·H** is stronger than the corresponding N−H in the arylamido product **6·H**. The additional driving force imparted through formation of a stronger amido bond in **5·H** is also consistent with faster HAT to **5**. There is also likely a steric contribution to the reactivity of **5** vs **6** because of the different size and shape of their imido *N*-substituents, although the

magnitude of the steric effect cannot be determined in the absence of a structure of **6**.

The HAT rate constant for $L^{Me,Ph3}$FeNAd (**5**) can also be compared to the reaction of $L^{Me,iPr2}$FeNAd with CHD (k = 1.4(2) × 10^{-4} M^{-1} s^{-1} at 10 °C),[9] which tests the effect of the choice of supporting β-diketiminate ligand on HAT rate. The imido complex **5** supported by $L^{Me,Ph3}$ abstracts H-atoms 2 orders of magnitude (143 ± 25 times) faster than the imido complex supported by $L^{Me,iPr2}$. The difference is probably not related to the change in electronic structure of the ligand, since the isopropyl → phenyl replacement occurs on *N*-aryl rings that are perpendicular to (i.e., not conjugated with) the diketiminate π-system. Since the isopropyl/phenyl groups are substituents on the *N*-aryl substituents, their inductive effect on the electronic structure at iron, and in turn on the reactive imido nitrogen, is expected to be negligible. If the effect on HAT rate is not electronic in nature, a reasonable alternative explanation is the steric properties of the two ligands affect the HAT transition state energy. However, explaining the steric difference between $L^{Me,Ph3}$ and $L^{Me,iPr2}$ is not trivial because isopropyl and phenyl groups are not the same shape. These considerations motivated the calculation of steric parameters that quantify the difference in overall ligand sterics between $L^{Me,Ph3}$ and $L^{Me,iPr2}$.

Diketiminate Size Comparisons. Various quantitative descriptors such as the classic Tolman cone angle[34] have been used to describe the "effective size" of ligands, helping chemists to understand how changes in ligand size or geometry affect reactivity. Recently, other measures have been introduced such as solid angles and the related *G* parameter,[35] which take into account the shape of the ligand in the calculation of size. The *G* parameter is defined as the fraction of surface area of a sphere of arbitrary radius that would be "shadowed" by the ligand if a light source was placed at the metal site (Figure 10).
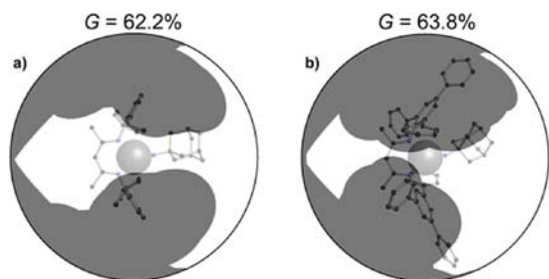
Figure 10. Visual representations of the ligand *G* parameters in (a) $L^{Me,iPr2}$FeNAd and (b) $L^{Me,Ph3}$FeNAd (**5**). The gray shaded area of the circumscribed sphere represents the shadow cast by the ligand when a light source is placed at the metal site (central sphere). Note that only one-half of each shadow is shown, with a similar shadow cast on the back half of the circumscribed sphere.

The *G* size parameter of **5** (63.8%) is only slightly larger than that for $L^{Me,iPr2}$FeNAd (62.2%), and so the ^{i}Pr → Ph substitution is a minimal *overall* change in size of the β-diketiminate ligand.[36] However, the *shape* of the flanking ligand arms (as seen by the shadows in Figure 10) offers a clearer explanation for the difference in HAT reactivity between **5** and $L^{Me,iPr2}$FeNAd. When the X-ray structures of **5** and $L^{Me,iPr2}$FeNAd are overlaid (Figure 11), the different orientation of the *N*-aryl groups with respect to the ligand backbone becomes apparent. While the 2,6-diisopropylphenyl substituent in $L^{Me,iPr2}$FeNAd is nearly 0.4° from perpendicular to the
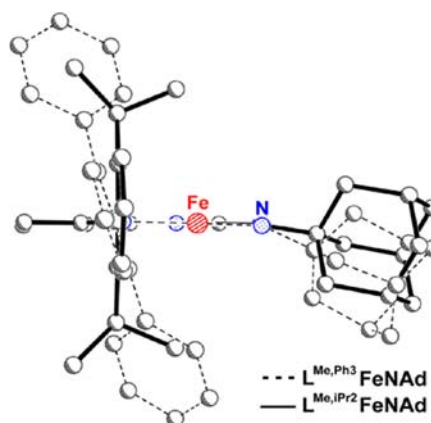
Figure 11. Overlay of $L^{Me,iPr2}$FeNAd (solid bonds) and **5** (dashed bonds) crystal structures highlighting the rotation of the *N*-aryl rings and bend of the Fe≡N−C linkage. Only one of each *N*-aryl group is shown for clarity.

diketiminate metallacycle, the 2,4,6-triphenylphenyl group in **5** is rotated 20.4° from perpendicular to the metallacycle. The result of this 2,4,6-triphenylphenyl rotation is to increase the amount of space directly above the imido nitrogen, which results in a larger binding pocket for hydrocarbon substrates (see the space-filling models in Figure 12). Therefore, we
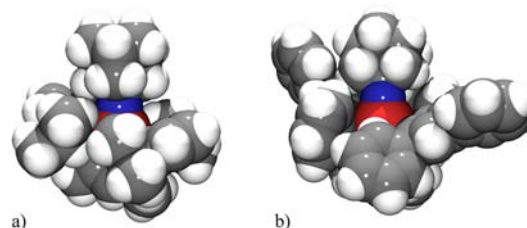
Figure 12. Spacefilling diagrams of (a) $L^{Me,iPr2}$FeNAd and (b) $L^{Me,Ph3}$FeNAd (**5**). Each diagram is oriented with the NAd group bent directly away.

reason that an incoming substrate would more easily attack the exposed imido nitrogen in **5** than the shielded imido nitrogen in $L^{Me,iPr2}$FeNAd, despite the overall larger shadowing of the $L^{Me,Ph3}$ ligand, because there is contiguous open space for approach of a hydrocarbon substrate.[37]

In addition to the roomier attack trajectory to the imide for incoming substrates, the increased rate of HAT for **5** may also be attributed to the change in the Fe≡N−R geometry. Compared to $L^{Me,iPr2}$FeNAd, complex **5** has a slightly longer Fe≡N bond (1.70 versus 1.67 Å) and significantly more bent Fe≡N−R angle (151° versus 170°). Computational studies of $L^{Me,iPr2}$FeNAd + CHD indicated that the transition state featured a lengthened Fe≡N bond (~1.9 Å) and more bent Fe≡N−R linkage (~140°) compared to the imido ground state geometry.[9] Thus, the faster HAT by **5** is consistent with an imido geometry that is closer to the transition state geometry, which would result in less structural reorganization needed to access the HAT transition state.

Interestingly, though the imido nitrogen atom is *more* exposed in **5**, the iron atom is *less* exposed. This is shown experimentally through the relative abilities of **5** and $L^{Me,iPr2}$FeNAd to coordinate pyridine at the iron center. Pyridine weakly coordinates to $L^{Me,iPr2}$FeNAd in the apical position of the trigonal plane[9] but not to **5**, whose iron center is

blocked by the flanking phenyl substituents. In this manner, the $L^{Me,Ph3}$ ligand *shields the iron* center but *exposes the imido nitrogen* to incoming substrates.

CONCLUSIONS

Iron-imido complexes of the 2,4,6-tri(phenyl)phenyl-substituted β-diketiminate ligand $L^{Me,Ph3}H$ are less susceptible to ligand C−H activation than the previously reported imido complex $L^{Me,iPr2}FeNAd$. The greater stability toward intramolecular decomposition led to the isolation of the first three-coordinate arylimidoiron complex. Despite the kinetic stability imparted by the $L^{Me,Ph3}$ ligand, the iron(III) imido complexes $L^{Me,Ph3}FeNMes$ and $L^{Me,Ph3}FeNAd$ are significantly more reactive (a factor of ~140) toward HAT than $L^{Me,iPr2}FeNAd$. The increase in HAT rate is explained by two observations: (1) a ligand N-aryl group rotates away from NAd in the crystal structure of $L^{Me,Ph3}FeNAd$, allowing more facile access of the substrate to the reactive nitrogen atom, and (2) the bent Fe=N−R linkage and lengthened Fe=N bond in $L^{Me,Ph3}FeNAd$ is closer to the expected transition-state geometry. It is notable that the $L^{Me,Ph3}$ ligand provides a larger substrate pocket for HAT than the $L^{Me,iPr2}$ ligand, despite the larger size of $L^{Me,Ph3}$. This highlights the importance of considering the overall shape of supporting ligands, in addition to the amount of coordination sphere coverage. In addition to these steric effects, the relative rates of HAT for arylimido and alkylimido complexes is consistent with imido basicity driving the HAT reaction. These studies illustrate the ability to modulate HAT reactivity with both steric and electronic changes to the ligands.

EXPERIMENTAL SECTION

General Considerations. All air-sensitive manipulations were performed under a nitrogen atmosphere in an MBraun glovebox maintained below 1 ppm of O_2 and H_2O, or on a double-manifold vacuum line using standard Schlenk techniques. For air-sensitive manipulations, all glassware was dried overnight at 150 °C. 1-Adamantyl azide was dissolved in pentane, filtered through Celite, and crystallized from pentane prior to use. Mesityl azide was prepared as previously described[38] and distilled under vacuum. 1,4-Cyclohexadiene was distilled from $CaCl_2$ and stored over activated 3 Å sieves. Anhydrous $FeBr_2$ was prepared from Fe and conc. HBr in MeOH, and dried at about 200 °C under vacuum for 12 h prior to use. Other reagents were obtained commercially and used without purification. Tetrahydrofuran (THF) was distilled from a purple sodium benzophenone ketyl solution, and other solvents were purified were by passage through activated alumina and "deoxygenizer" columns from Glass Contour Co. Benzene-d_6 was dried over flame-activated alumina. Before use, an aliquot of each solvent was tested with a drop of THF containing sodium benzophenone ketyl to qualitatively ensure dryness. NMR data were collected on either a Bruker Avance 400 or Bruker Avance 500 spectrometer. ^{1}H NMR spectra are referenced to residual C_6D_5H (δ 7.16 ppm), C_7D_7H (δ 2.08 ppm), or TMS (δ 0.00 ppm). ^{13}C NMR spectra were referenced to $CDCl_3$ (δ 77.16 ppm) or C_6D_6 (δ 128.06 ppm). Mass spectral data were obtained on a Shimadzu QP2010 system with electron impact ionization. IR data were recorded on a Shimadzu 8400S FTIR spectrometer using pressed KBr sample pellets. UV−vis data were recorded on a Cary 50 spectrometer using Schlenk-adapted cuvettes. The emission spectrum of **2** was recorded on a Spex Fluoromax-P fluorimeter with a photomultiplier tube detector. Elemental analyses were determined at the CENTC Elemental Analysis Facility using a PerkinElmer 2400 Series II Analyzer with sample capsules prepared under argon. Solution magnetic susceptibilities were determined by the Evans method.[39]

2,4,6-Triphenylaniline. A 1000-mL flask was loaded with 2,4,6-triphenylnitrobenzene (20.5 g, 58 mmol) and ^{i}PrOH (400 mL), giving a white slurry. Dry 10% Pd/C (3.1 g, 2.9 mmol of Pd) was treated with

water (10 mL), and the slurry was added to the reaction flask. The flask was evacuated and backfilled with a H_2 balloon, and the mixture was heated in an 80 °C oil bath. When the reaction was complete by TLC (ca. 14 h) the hot mixture was filtered through Celite and allowed to cool to room temperature, at which point the product began to crystallize from the filtrate. The mixture was cooled to −25 °C, and 14.2 g of fluffy crystalline solid was collected by filtration. An additional crop of crystals (2.7 g) was obtained by concentrating the supernatant and storing at −25 °C. Combined yield: 16.9 g (90%). ^{1}H NMR ($CDCl_3$): δ 7.56−7.61 (m, 6H), 7.48 (t, 4H), 7.41 (s, 2H), 7.38 (m, 4H), 7.27 (d, 1H), 3.91 (s, 2H, NH_2) ppm. The NMR spectrum is identical to literature data.[40]

2,4-Bis(2,4,6-triphenylphenylimido)pentane ($L^{Me,Ph3}H$) (1). A 500-mL flask was loaded with 2,4,6-triphenylaniline (16.1 g, 50.2 mmol), *p*-toluenesulfonic acid monohydrate (4.77 g, 25.1 mmol), 2,4-pentanedione (2.56 mL, 25.1 mmol), and xylenes (350 mL). The mixture was sparged with N_2, and the flask was fitted with a Dean−Stark condenser. The mixture was heated in a 160 °C oil bath for 24 h. Most of the volatile materials were removed under vacuum, affording a brown gooey solid. Aqueous Na_2CO_3 (300 mL) and CH_2Cl_2 (300 mL) were added to the residue, and the mixture was vigorously stirred for 30 min. The organic layer was removed and washed with brine (2 × 300 mL) and dried over $MgSO_4$. The solution was concentrated to ~150 mL, and MeOH was added until the solution just became cloudy (~75 mL). Upon standing, dark yellow crystals deposited, which were isolated by filtration. The crystals were ground into a fine yellow powder and heated under vacuum at 120 °C for 12 h to ensure complete removal of cocrystallized solvent. Yield = 10.60 g. A second crop of crystals (2.54 g) was obtained by adding more MeOH to the supernatant (~100 mL), affording a total yield of $L^{Me,Ph3}H$ of 13.14 g (74%). ^{1}H NMR ($CDCl_3$, 400 MHz): δ 12.2 (s, 1H, NH), 7.70 (d, J = 7.4 Hz, 4H), 7.58 (s, 4H), 7.44 (t, J = 7.6 Hz, 4H), 7.34 (t, J = 7.4 Hz, 2H), 7.11−7.21 (m, 20H), 4.14 (s, 1H, α-CH), 1.24 (s, 6H, CH_3) ppm. ^{13}C{^{1}H} NMR ($CDCl_3$, 101 MHz): δ 160.0 (C=N), 141.0 (C_{ipso}), 140.6 (C_{ipso}), 140.2 (C_{ipso}), 137.3 (C_{ipso}), 136.7 (C_{ipso}), 129.4 (C_{Ar}−H), 128.9 (C_{Ar}−H), 128.5 (C_{Ar}−H), 128.2 (C_{Ar}−H), 127.2 (C_{Ar}−H), 127.0 (C_{Ar}−H), 126.9 (C_{Ar}−H), 126.8 (C_{Ar}−H), 96.7 (α-CH), 21.2 (CH_3) ppm. IR (thin film): 3582 (w, ν_{N-H}), 3079 (w), 3055 (m), 3027 (m), 2920 (w), 1622 (s), 1597 (m), 1544 (s), 1494 (m), 1454 (m), 1421 (s), 1397 (m), 1377 (m), 1362 (m), 1278 (m), 1179 (m), 1070 (w), 1029 (m), 887 (m), 754 (s), 733 (m) cm^{-1}. UV−vis (CH_2Cl_2) (λ_{max} (ε in mM^{-1} cm^{-1})): 251 (77), 377 (25). Elem. Anal. Calcd. for $C_{53}H_{42}N_2$: C 90.05; H 5.99; N 3.96. Found: C 89.91; H 6.10; N 4.01.

$L^{Me,Ph3}Li(OEt_2)$ (2). A Schlenk flask was loaded with $L^{Me,Ph3}H$ (2.15 g, 3.04 mmol) and diethyl ether (100 mL) to give a yellow mixture. A solution of ^{n}BuLi (1.22 mL of a 2.5 M solution in hexane, 3.04 mmol) was added slowly at room temperature. Upon addition of the ^{n}BuLi, the mixture developed a cyan-colored fluorescence. The mixture was stirred for 4 h, and the volatile materials were removed under vacuum to afford an amorphous yellow solid. The solid was slurried in pentane (~50 mL), and collected on a glass fritted funnel. The yellow powder was dried under vacuum, affording 2.18 g (91%) of $L^{Me,Ph3}Li(OEt_2)$. ^{1}H NMR (C_6D_6): δ 7.68 (s, 4H), 7.52 (d, J = 7.6 Hz, 4H), 7.43 (d, J = 7.6 Hz, 8H), 7.35 (t, J = 7.6 Hz, 8H), 7.21 (t, J = 7.6 Hz, 4H), 7.15 (s, 2H), 7.14 (t, J = 7.6 Hz, 4H), 4.43 (s, 1H, α-CH), 2.68 (q, J = 6.8, 4H, O(CH_2CH$_3$)$_2$), 1.60 (s, 6H, CH$_3$), 0.27 (t, J = 6.8, 6H, O(CH$_2$CH_3)$_2$) ppm. ^{13}C{^{1}H} NMR (C_6D_6, 101 MHz): δ 164.5 (C=N), 149.3 (C_{ipso}), 142.4 (C_{ipso}), 141.4 (C_{ipso}), 136.5 (C_{ipso}), 135.4 (C_{ipso}), 130.5 (C_{Ar}−H), 130.2 (C_{Ar}−H), 130.0 (C_{Ar}−H), 129.7 (C_{Ar}−H), 129.5 (C_{Ar}−H), 129.1 (C_{Ar}−H), 127.1 (C_{Ar}−H), 126.8 (C_{Ar}−H), 126.6 (C_{Ar}−H), 126.3 (C_{Ar}−H), 96.2 (α-CH), 66.0 (OCH_2CH$_3$), 24.7 (N=C−CH_3), 13.0 (OCH$_2$$CH_3$) ppm. UV−vis (Et$_2$O) ($\lambda_{max}$ (ε in mM^{-1} cm^{-1})): 255 (54), ~290 (sh, ~15), 418 (27). Elem. Anal. Calcd. for $C_{57}H_{51}LiN_2O$: C 86.99; H 6.53; N 3.56. Found: C 86.37; H 6.79; N 3.43.

$[L^{Me,Ph3}Fe(\mu-Br)]_2$ (3). A Schlenk flask was loaded with $FeBr_2$ (0.604 g, 2.80 mmol) and THF (30 mL), and a solution of $L^{Me,Ph3}Li(OEt_2)$ (2.20 g, 2.80 mmol) in THF (30 mL) was added, giving a yellow-brown mixture. The mixture was stirred at room

8358

dx.doi.org/10.1021/ic300870y | *Inorg. Chem.* 2012, 51, 8352−8361

temperature for 14 h, and the volatile materials were removed under vacuum. The solid was heated under vacuum (100 °C for 3 h) until the solid changed color to orange-red. Toluene (100 mL) was added, and the solution was filtered through a pad of Celite, and the volatile materials were removed under vacuum. The orange solid was washed with pentane (50 mL) and dried under vacuum to afford $[L^{Me,Ph3}Fe(\mu\text{-}Br)]_2$ (2.12 g, 90%). ^{1}H NMR (CD_2Cl_2): δ 29.0, 12.1, 7.3, 0.0, −2.5, −4.4, −9.1, −13.4, −14.2, −16.3, −25.5, −38.5 ppm. In CD_2Cl_2, the peaks were very broad and overlapped, preventing accurate integration. ^{1}H NMR (THF-d_8): δ 20.5 (4H, Ar−H), 8.6 (4H, Ar−H), 0.0 (2H, Ar−H), −0.3 (8H, Ar−H), −0.9 (4H, Ar−H), −1.3 (4H, Ar−H), −13.3 (8H, Ar−H), −24.4 (1H, backbone C−H), −35.4 (6H, CH_3). UV−vis (CH_2Cl_2) (λ_{max} (ε in mM^{-1} cm^{-1})): 251 (160), 349 (33), ~390 (sh, ~20), 536 (0.82). μ_{eff} (CD_2Cl_2, 23 °C): 7.5(4) μ_B. Elem. Anal. Calcd. for $C_{106}H_{82}Br_2Fe_2N_4$: C 75.63; H 4.91; N 3.33. Found: C 75.72; H 5.14; N 3.39.

$L^{Me,Ph3}$Fe (4). A 20-mL scintillation vial was loaded with $[L^{Me,Ph3}Fe(\mu\text{-}Br)]_2$ (578 mg, 0.34 mmol) and diethyl ether (~12 mL). KC_8 (93 mg, 0.69 mmol) was added in portions over 1 min, and the mixture immediately turned dark red-brown. The mixture was stirred for 4 h and filtered through Celite. The filter cake was washed with Et_2O until the washes were colorless (~200 mL), and the resulting solution was dried under vacuum to afford a dark red-brown solid (464 mg, 89%). ^{1}H NMR (C_6D_{12}): no peaks. EPR (2-MeTHF, 50 K): g = 2.186, 2.102, 1.980. IR (KBr): 3055 (w), 3028 (w), 2960 (w), 2923 (w), 1597 (w), 1523 (m), 1493 (w), 1423 (m), 1379 (vs), 1361 (s), 1342 (w), 1277 (w), 1258 (w), 1185 (m), 1072 (w), 1022 (w), 887 (w), 798 (w), 758 (s), 698 (s), 624 (m) cm^{-1}. UV−vis (THF) (λ_{max} (ε in mM^{-1} cm^{-1})): 209 (92), 252 (76), 364 (17), 451 (5.1), 541 (2.4), ~610(sh) (~1), 878 (0.17). μ_{eff} (C_6D_{12}, 25 °C): 1.8(1) μ_B. Elem. Anal. Calcd. for $C_{53}H_{41}FeN_2$: C 83.57; H 5.43; N 3.68. Found: C 84.22; H 5.79; N 3.54.

$L^{Me,Ph3}$FeNAd (5). A 20-mL scintillation vial was loaded with $L^{Me,Ph3}$Fe (232 mg, 0.304 mmol) and benzene (~8 mL). With vigorous stirring, a solution of N_3Ad (54 mg, 0.31 mmol) in benzene (~1 mL) was added, causing effervescence and a subtle color change to lighter brown. The mixture was stirred 30 min, and the volatile materials were removed under vacuum. The resulting brown solid was triturated with a small amount of Et_2O until solid began to crystallize. The mixture was stored overnight at −45 °C, affording $L^{Me,Ph3}$FeNAd (115 mg, 42%). ^{1}H NMR (C_6D_6): δ 73.8 (6H, CH_3 or Ad-H), 43.2 (1H, backbone C−H), 32.5 (3H, Ad-H), 30.4 (Ad-H), 27.3 (3H, Ad-H), 4.8 (4H, Ar−H), 2.0 (2H, Ar−H), −0.8 (4H, Ar−H), −3.0 (4H, Ar−H), −5.7 (8H, Ar−H), −10.0 (4H, Ar−H), −22.5 (6H, CH_3 or Ad-H), −35.5 (8H, Ar−H) ppm. EPR (toluene, 8 K): g_{eff} = 7.11, 1.55, 1.26. μ_{eff} (C_6D_6, 25 °C): 4.0(2) μ_B. Small impurities were evident by ^{1}H NMR spectroscopy, which prevented elemental analysis.

$L^{Me,Ph3}$FeNMes (6). A 20-mL scintillation vial was loaded with $L^{Me,Ph3}$Fe (51 mg, 67 μmol) and benzene (~3 mL). With vigorous stirring, a solution of N_3Mes (10 μL, 67 μmol) in benzene (~1 mL) was added dropwise, causing effervescence and a subtle color change to reddish brown. The mixture was stirred 30 min, and the volatile materials were removed under vacuum. The resulting brown solid was crystallized from toluene, affording $L^{Me,Ph3}$FeNMes (37 mg, 61%). ^{1}H NMR (C_6D_6): δ 50.1 (1H, backbone C−H), 42.9 (2H, Ar−H or Mes-H), 6.6 (2H, Ar−H or Mes-H), 4.4 (4H, Ar−H), 2.0 (8H, Ar−H), −4.8 (8H + 3H, Ar−H + Mes-CH_3), −6.1 (4H, Ar−H), −7.1 (4H, Ar−H), −21.4 (6H, backbone CH_3 or Mes-CH_3), −28.3 (6H, backbone CH_3 or Mes-CH_3), −59.3 (4H, Ar−H) ppm. EPR (toluene, 8 K): g_{eff} = 7.42, 1.03, 0.89. μ_{eff} (C_6D_6, 25 °C): 4.1(3) μ_B. Small impurities were evident by ^{1}H NMR spectroscopy, which prevented elemental analysis.

$L^{Me,Ph3}$FeNHMes (6·H). A 20-mL scintillation vial was loaded with a solution of freshly distilled $MesNH_2$ (19.6 mg, 0.145 mmol) and THF (2 mL). A solution of ^nBuLi in hexane (58 μL of a 2.5 M solution, 0.150 mmol) was added, and the mixture was stirred for 10 min. This solution was added to a solution of $[L^{Me,Ph3}Fe(\mu\text{-}Br)]_2$ (122 mg, 0.072 mmol) in THF (5 mL), which caused a color change from yellow to orange-red. The mixture was stirred 10 min, and the volatile materials were removed under vacuum. The resulting orange-red solid

was crystallized by vapor diffusion of pentane into a saturated toluene solution at room temperature, affording dark red crystals of $L^{Me,Ph3}$FeNHMes (97 mg, 75%). ^{1}H NMR (C_6D_6): δ 120 (6H, backbone CH_3 or Mes-CH_3), 118 (4H, Ar−H), 91.7 (2H, Ar−H or Mes-H), 63.3 (1H, backbone C−H), 16.5 (6H, backbone CH_3 or Mes-CH_3), 6.5 (4H, Ar−H), 4.6 (4H, Ar−H), 4.2 (4H, Ar−H), −0.5 (2H, Ar−H or Mes-H), −8.4 (3H, Mes-CH_3), −9.3 (8H, Ar−H), −13.2 (4H, Ar−H), −38.0 (8H, Ar−H). Elem. Anal. Calcd. for $C_{62}H_{53}FeN_3$: C 83.11; H 5.96; N 4.69. Found: C 82.79; H 6.11; N 4.68.

^{1}H NMR Kinetics. A general procedure for the HAT reaction kinetics is given. A J. Young NMR tube was loaded with 0.4 mL of a 15 mM stock solution of **5** in C_6D_6 and an integration standard (a sealed capillary of cobaltocene in C_7D_8), and the tube was sealed with a rubber septum. The tube was chilled in an ice bath (~0 °C), and 1,4-cyclohexadiene was added via microsyringe. The tube was quickly shaken and immediately inserted into the NMR probe which was precooled to 10 °C (probe temperature calibrated using neat ethylene glycol or methanol[41]). A kinetic acquisition program was started immediately, and spectra were recorded every 50 s until the reaction was >95% complete. The plot of integration of **5** versus time was fit to a first-order exponential equation $y = A + B \cdot \exp(-k_{obs} \cdot t)$, where A and B are constants and k_{obs} is the pseudo-first-order rate constant.

Crystallography. Crystals were placed onto the tip of a ~0.1 mm diameter glass fiber and mounted on a Bruker SMART APEX II CCD Platform diffractometer[42] for a data collection at 100.0(1) K (except compound **4** at 103(5) K) using MoKα radiation and a graphite monochromator. Randomly oriented regions of reciprocal space were surveyed: four major sections of frames were collected with 0.50° steps in ω at four different ϕ settings and a detector position of −33° in 2θ. The intensity data were corrected for absorption.[43] Final cell constants were calculated from the xyz centroids of about 4000 strong reflections from the actual data collection. The structures were solved using SIR97[44] and refined using SHELXL-97.[45] The space groups were determined by systematic absences and intensity statistics. All non-hydrogen atoms were refined with anisotropic displacement parameters, and hydrogen atoms were placed in ideal positions and refined as riding atoms with relative isotropic displacement parameters (except the amido hydrogen in compound **6·H** described below). For compound **1**, two peaks of remaining electron density (~0.9 $e \cdot Å^{-3}$ each) were located near the aryl ring C72 → C102. The distance between these peaks of 2.89 Å is consistent with the Cl−Cl distance in CH_2Cl_2, thus suggesting trace occupancy by a dichloromethane molecule. When these density peaks were included in the refinement model, occupancy of the Cl positions refined to ~0.04 (i.e., 4%). This did not significantly improve the overall model and its statistics; thus the dichloromethane was omitted from the final model. Additionally, two connected aryl rings were modeled as disordered over two positions (88:12). For compound **4**, two of the three cocrystallized toluene solvent molecules lie on crystallographic inversion centers and were modeled as disordered over the centers (50:50, by symmetry). For compound **5**, highly disordered solvent was found around a crystallographic inversion center that could not be identified or refined. Reflection contributions from this solvent were removed using program PLATON, function SQUEEZE,[46] which determined there to be 144 electrons in 432 Å^3 removed per unit cell. Since the exact identity and quantity of the solvent was unknown, it was not included in the molecular formula. Thus all fields that derive from the molecular formula (e.g., $F(000)$, calculated density) are known to be incorrect. For compound **6·H**, the amido hydrogen atom H14 was found from the difference Fourier map, and its positional and isotropic displacement parameters were refined independently from those of its bonded nitrogen atom. Full crystallographic refinement details are given in the Supporting Information.

ASSOCIATED CONTENT

S **Supporting Information**

Additional kinetic, crystallographic, and spectral data. This material is available free of charge via the Internet at http://pubs.acs.org.

AUTHOR INFORMATION

Corresponding Author

*E-mail: holland@chem.rochester.edu.

Notes

The authors declare no competing financial interest.

ACKNOWLEDGMENTS

REFERENCES

(1) (a) Hodgkiss, J. M.; Rosenthal, J.; Nocera, D. G. The Relation between Hydrogen Atom Transfer and Proton-coupled Electron Transfer in Model Systems. In *Hydrogen-Transfer Reactions*; Hynes, J. T., Klinman, J. P., Limbach, H.-H., Schowen, R. L., Eds.; Wiley-VCH: Weinheim, Germany, 2007; Vol. 2, pp 503−562. (b) Schöneich, C. Hydrogen Atom Transfer in Model Reactions. In *Hydrogen-Transfer Reactions*; Hynes, J. T., Klinman, J. P., Limbach, H.-H., Schowen, R. L., Eds.; Wiley-VCH: Weinheim, Germany, 2007; Vol. 3, pp 1013−1036. (c) Mayer, J. M. *Annu. Rev. Phys. Chem.* **2004**, *55*, 363−390. (d) Hammes-Schiffer, S. *ChemPhysChem* **2002**, *3*, 33−42. (e) Huynh, M. H. V.; Meyer, T. J. *Chem. Rev.* **2007**, *107*, 5004−5064. (f) Warren, J. J.; Tronic, T. A.; Mayer, J. M. *Chem. Rev.* **2010**, *110*, 6961−7001.

(2) Gunay, A.; Theopold, K. H. *Chem. Rev.* **2010**, *110*, 1060−1081.

(3) (a) Ortiz de Montellano, P. R., Ed.; *Cytochrome P-450: Structure, Mechanism and Biochemistry*, 3rd ed.; Plenum Publishers: New York, 2005. (b) Sono, M.; Roach, M. P.; Coulter, E. D.; Dawson, J. H. *Chem. Rev.* **1996**, *96*, 2841−2888. (c) Meunier, B.; de Visser, S. P.; Shaik, S. *Chem. Rev.* **2004**, *104*, 3947−3980. (d) Ragsdale, S. W. *Chem. Rev.* **2006**, *106*, 3317−3337. (e) Baik, M.-H.; Newcomb, M.; Friesner, R. A.; Lippard, S. J. *Chem. Rev.* **2003**, *103*, 2385−2419. (f) Stubbe, J.; Nocera, D. G.; Yee, C. S.; Chang, M. C. Y. *Chem. Rev.* **2003**, *103*, 2167−2201. (g) Hydrogen Atom Transfers in B$_{12}$ Enzymes. In *Hydrogen-Transfer Reactions*; Hynes, J. T., Klinman, J. P., Limbach, H.-H., Schowen, R. L., Eds.; Wiley-VCH: Weinheim, Germany, 2007; Vol. 4, pp 1473−1495. (h) Liang, Z.-X.; Klinman, J. P. *Curr. Opin. Struct. Biol.* **2004**, *14*, 648−655. (i) Baldwin, J. E.; Bradley, M. *Chem. Rev.* **1990**, *90*, 1079−1088. (j) Schenk, W. A. *Angew. Chem., Int. Ed.* **2000**, *39*, 3409−3411. (k) Krebs, C.; Fujimori, D. G.; Walsh, C. T.; Bollinger, J. M. *Acc. Chem. Res.* **2007**, *40*, 484−492. (l) Solomon, E. I.; Brunold, T. C.; Davis, M. I.; Kemsley, J. N.; Lee, S.-K.; Lehnert, N.; Neese, F.; Skulan, A. J.; Yang, Y.-S.; Zhou, J. *Chem. Rev.* **2000**, *100*, 235−349.

(4) (a) Sastri, C. V.; Lee, J.; Oh, K.; Lee, Y. J.; Lee, J.; Jackson, T. A.; Ray, K.; Hirao, H.; Shin, W.; Halfen, J. A.; Kim, J.; Que, L.; Shaik, S.; Nam, W. *Proc. Natl. Acad. Sci. U. S. A.* **2007**, *104*, 19181−19186. (b) Paine, T. K.; Costas, M.; Kaizer, J.; Que, L. *J. Biol. Inorg. Chem.* **2006**, *11*, 272−276. (c) Que, L.; Tolman, W. B. *Nature* **2008**, *455*, 333−340. (d) Ray, K.; England, J.; Fiedler, A. T.; Martinho, M.; Münck, E.; Que, L. *Angew. Chem., Int. Ed.* **2008**, *47*, 8068−8071. (e) Decker, A.; Rohde, J.-U.; Klinker, E. J.; Wong, S. D.; Que, L.; Solomon, E. I. *J. Am. Chem. Soc.* **2007**, *129*, 15983−15996. (f) Fiedler, A. T.; Que, L. *Inorg. Chem.* **2009**, *48*, 11038−11047. (g) Klinker, E. J.; Shaik, S.; Hirao, H.; Que, L. *Angew. Chem., Int. Ed.* **2009**, *48*, 1291−1295. (h) England, J.; Martinho, M.; Farquar, E. R.; Frisch, J. R.;

Bominaar, E. L.; Münck, E.; Que, L. *Angew. Chem., Int. Ed.* **2009**, *48*, 3622−3626. (i) Kaizer, J.; Klinker, E. J.; Oh, N. Y.; Rohde, J.-U.; Song, W. J.; Stubna, A.; Kim, J.; Münck, E.; Nam, W.; Que, L. *J. Am. Chem. Soc.* **2004**, *126*, 472−473. (j) Jeong, Y. J.; Kang, Y.; Han, A.-R.; Lee, Y.-M.; Kotani, H.; Fukuzumi, S.; Nam, W. *Angew. Chem., Int. Ed.* **2008**, *47*, 7321−7324. (k) Kang, Y.; Chen, H.; Jeong, Y. J.; Lai, W.; Bae, E. H.; Shaik, S.; Nam, W. *Chem.—Eur. J.* **2009**, *15*, 10039−10046. (l) Fujii, H. *Coord. Chem. Rev.* **2002**, *226*, 51−60. (m) Jin, N.; Groves, J. T. *J. Am. Chem. Soc.* **1999**, *121*, 2923−2924. (n) Lansky, D. E.; Goldberg, D. P. *Inorg. Chem.* **2006**, *45*, 5119−5125. (o) Bryant, J. R. *J. Am. Chem. Soc.* **2003**, *125*, 10351−10361. (p) Bryant, J. R.; Green, M. T.; Matsuo, T.; Mayer, J. M. *Inorg. Chem.* **2004**, *43*, 1587−1592. (q) Matsuo, T.; Mayer, J. M. *Inorg. Chem.* **2005**, *44*, 2150−2158. (r) Cook, G. K.; Mayer, J. M. *J. Am. Chem. Soc.* **1994**, *116*, 1855−1868. (s) Cook, G. K.; Mayer, J. M. *J. Am. Chem. Soc.* **1995**, *117*, 7139−7156. (t) Waidmann, C. R.; Zhou, X.; Tsai, E. A.; Kaminsky, W.; Hrovat, D. A.; Borden, W. T.; Mayer, J. M. *J. Am. Chem. Soc.* **2009**, *131*, 4729−4743. (u) Gardner, K. A.; Mayer, J. M. *Science* **1995**, *269*, 1849−1851. (v) Gardner, K. A.; Kuehnert, L. L.; Mayer, J. M. *Inorg. Chem.* **1997**, *36*, 2069−2078. (w) Parsell, T. H.; Behan, R. K.; Green, M. P.; Hendrich, M. P.; Borovik, A. S. *J. Am. Chem. Soc.* **2006**, *128*, 8728−8729. (x) Parsell, T. H.; Yang, M.-Y.; Borovik, A. S. *J. Am. Chem. Soc.* **2009**, *131*, 2762−2763. (y) Gupta, R.; Borovik, A. S. *J. Am. Chem. Soc.* **2003**, *125*, 13234−13242. (z) Seok, W. K.; Meyer, T. J. *Inorg. Chem.* **2005**, *44*, 3931−3941. (aa) Binstead, R. A.; McGuire, M. E.; Dovletoglou, A.; Seok, W. K.; Roecker, L. E.; Meyer, T. J. *J. Am. Chem. Soc.* **1992**, *114*, 173−186. (bb) Gilbert, J. A.; Gersten, S. W.; Meyer, T. J. *J. Am. Chem. Soc.* **1982**, *104*, 6872−6873. (cc) Gilbert, J. A.; Roecker, L.; Meyer, T. J. *Inorg. Chem.* **1987**, *26*, 1126−1132. (dd) Binstead, R. A.; Meyer, T. J. *J. Am. Chem. Soc.* **1987**, *109*, 3287−3297. (ee) Binstead, R. A.; Moyer, B. A.; Samuels, G. J.; Meyer, T. J. *J. Am. Chem. Soc.* **1981**, *103*, 2897−2899.

(5) Observed HAT reactions to imido ligands: (a) Kogut, E.; Wiencko, H. L.; Zhang, L.; Cordeau, D. E.; Warren, T. H. *J. Am. Chem. Soc.* **2005**, *127*, 11248−11249. (b) Iluc, V. M.; Hillhouse, G. L. *J. Am. Chem. Soc.* **2010**, *132*, 15148−15150. (c) Iluc, V. M.; Miller, A. J. M.; Anderson, J. S.; Monreal, M. J.; Mehn, M. P.; Hillhouse, G. L. *J. Am. Chem. Soc.* **2011**, *133*, 13055−13063. (d) Wiese, S.; McAfee, J. L.; Pahls, D. R.; McMullin, C. L.; Cundari, T. R.; Warren, T. H. *J. Am. Chem. Soc.* **2012**, *134*, 10114−10121.

(6) Reactions of imido complexes that implicate HAT: (a) Jensen, M. P.; Mehn, M. P.; Que, L., Jr. *Angew. Chem., Int. Ed.* **2003**, *42*, 4357−4360. (b) Thyagarajan, S.; Shay, D. T.; Incarvito, C. D.; Rheingold, A. L.; Theopold, K. H. *J. Am. Chem. Soc.* **2003**, *125*, 4440−4441. (c) Shay, D. T.; Yap, G. P. A.; Zakharov, L. N.; Rheingold, A. L.; Theopold, K. H. *Angew. Chem., Int. Ed.* **2005**, *44*, 1508−1510. (d) Lucas, R. L.; Powell, D. R.; Borovik, A. S. *J. Am. Chem. Soc.* **2005**, *127*, 11596−11597. (e) Badiei, Y. M.; Dinescu, A.; Dai, X.; Palomino, R. M.; Heinemann, F. W.; Cundari, T. R.; Warren, T. H. *Angew. Chem., Int. Ed.* **2008**, *47*, 9961−9964. (f) Ni, C.; Fettinger, J. C.; Long, G. J.; Brynda, M.; Power, P. P. *Chem. Commun.* **2008**, 6045−6047. (g) Avenier, F.; Gouré, E.; Dubourdeaux, P.; Sénèque, O.; Oddou, J.-L.; Pécaut, J.; Chardon-Noblat, S.; Deronzier, A.; Latour, J.-M. *Angew. Chem., Int. Ed.* **2008**, *47*, 715−717. (h) Chomitz, W. A.; Arnold, J. *Chem. Commun.* **2008**, 3648−3650. (i) King, E. R.; Betley, T. A. *Inorg. Chem.* **2009**, *48*, 2361−2363. (j) Fantauzzi, S.; Gallo, E.; Caselli, A.; Ragaini, F.; Casati, N.; Macchi, P.; Cenini, S. *Chem. Commun.* **2009**, 3952−3954. (k) Mankad, N. P.; Müller, P.; Peters, J. C. *J. Am. Chem. Soc.* **2010**, *132*, 4083−4085.

(7) Cowley, R. E.; DeYonker, N. J.; Eckert, N. A.; Cundari, T. R.; DeBeer, S.; Bill, E.; Ottenwaelder, X.; Flaschenriem, C.; Holland, P. L. *Inorg. Chem.* **2010**, *49*, 6172−6187.

(8) Eckert, N. A.; Vaddadi, S.; Stoian, S.; Lachicotte, R. J.; Cundari, T. R.; Holland, P. L. *Angew. Chem., Int. Ed.* **2006**, *45*, 6868−6871.

(9) Cowley, R. E.; Eckert, N. A.; Vaddadi, S.; Figg, T. M.; Cundari, T. R.; Holland, P. L. *J. Am. Chem. Soc.* **2011**, *133*, 9796−9811.

(10) Cowley, R. E.; Holland, P. L. *Inorg. Chim. Acta* **2011**, *369*, 40−44.

(11) The abbreviations used in this paper for the β-diketiminate ligands are of the form $L^{R,R'}$, where R represents the substituent on the backbone imine carbons, and R' represents the identity and number of substituents on the N-aryl rings.

(12) Mindiola, D. J.; Holland, P. L.; Warren, T. H. *Inorg. Synth.* **2010**, *35*, 1−4.

(13) Stender, M.; Wright, R. J.; Eichler, B. E.; Prust, J.; Olmstead, M. M.; Roesky, H. W.; Power, P. P. *J. Chem. Soc., Dalton Trans.* **2001**, 3465−3469.

(14) Budzelaar, P. H. M.; van Oort, A. B.; Orpen, A. G. *Eur. J. Inorg. Chem.* **1998**, 1485−1494.

(15) Vidovic, D.; Jones, J. N.; Moore, J. A.; Cowley, A. H. *Z. Anorg. Allg. Chem.* **2005**, *631*, 2888−2892.

(16) Tonzetich, Z. J.; Héroguel, F.; Do, L. H.; Lippard, S. J. *Inorg. Chem.* **2011**, *50*, 1570−1579.

(17) Vela, J.; Cirera, J.; Smith, J. M.; Lachicotte, R. J.; Flaschenriem, C. J.; Alvarez, S.; Holland, P. L. *Inorg. Chem.* **2007**, *46*, 60−71.

(18) Chiang, K. P.; Barrett, P. M.; Ding, F.; Smith, J. M.; Kingsley, S.; Brennessel, W. W.; Clark, M. M.; Lachicotte, R. J.; Holland, P. L. *Inorg. Chem.* **2009**, *48*, 5106−5116.

(19) (a) Smith, J. M.; Lachicotte, R. J.; Pittard, K. A.; Cundari, T. R.; Lukat-Rodgers, G.; Rodgers, K. R.; Holland, P. L. *J. Am. Chem. Soc.* **2001**, *123*, 9222−9223. (b) Smith, J. M.; Sadique, A. R.; Cundari, T. R.; Rodgers, K. R.; Lukat-Rodgers, G.; Lachicotte, R. J.; Vela, J.; Holland, P. L. *J. Am. Chem. Soc.* **2006**, *128*, 756−769.

(20) Rodriguez, M. M.; Bill, E.; Brennessel, W. W.; Holland, P. L. *Science* **2011**, *334*, 780−783.

(21) Dugan, T. R.; Sun, X.; Rybak-Akimova, E. V.; Olatunji-Ojo, O.; Cundari, T. R.; Holland, P. L. *J. Am. Chem. Soc.* **2011**, *133*, 12418−12421.

(22) Amisial, L. D.; Dai, X.; Kinney, R. A.; Krishnaswamy, A.; Warren, T. H. *Inorg. Chem.* **2004**, *43*, 6537−6539.

(23) Pfirrmann, S.; Yao, S.; Ziemer, B.; Stösser, R.; Driess, M.; Limberg, C. *Organometallics* **2009**, *28*, 6855−6860.

(24) Chang, K.-C.; Lu, C.-F.; Wang, P.-Y.; Lu, D.-Y.; Chen, H.-Z.; Kuo, T.-S.; Tsai, Y.-C. *Dalton Trans.* **2011**, *40*, 2324−2331.

(25) Yu, Y.; Sadique, A. R.; Smith, J. M.; Dugan, T. R.; Cowley, R. E.; Brennessel, W. W.; Flaschenriem, C. J.; Bill, E.; Cundari, T. R.; Holland, P. L. *J. Am. Chem. Soc.* **2008**, *130*, 6624−6638.

(26) Cowley, R. E.; Eckert, N. A.; Elhaïk, J.; Holland, P. L. *Chem. Commun.* **2009**, 1760−1762.

(27) Sadique, A. R.; Brennessel, W. W.; Holland, P. L. *Inorg. Chem.* **2008**, *47*, 784−786.

(28) Cowley, R. E.; Elhaïk, J.; Eckert, N. A.; Brennessel, W. W.; Bill, E.; Holland, P. L. *J. Am. Chem. Soc.* **2008**, *130*, 6074.

(29) Smith, J. M.; Lachicotte, R. J.; Holland, P. L. *J. Am. Chem. Soc.* **2003**, *125*, 15752−15753.

(30) There are two possibilities for the second HAT event after the generation of 1,4-cyclohexadienyl radical (CHD$^{\bullet}$): either (*i*) a second imide performs HAT from CHD$^{\bullet}$ (calculated C−H BDE = 22 kcal/mol, see: Gao, Y.; DeYonker, N. J.; Garrett, E. C.; Wilson, A. K.; Cundari, T. R.; Marshall, P. *J. Phys. Chem. A* **2009**, *113*, 6955−6963.) to form benzene directly; or (*ii*) CHD$^{\bullet}$ disproportionates to CHD and benzene, and the second imide performs HAT from additional CHD (radical disproportionation can be fast under certain conditions, see: Arends, I. W. C. E.; Mulder, P.; Clark, K. B.; Wayner, D. D. M. *J. Phys. Chem.* **1995**, *99*, 8182−8189). These possibilities give identical byproduct (0.5 equiv of benzene) and are kinetically indistinguishable

(31) (a) Green, M. T.; Dawson, J. H.; Gray, H. B. *Science* **2004**, *304*, 1653−1656. (b) Behan, R. K.; Hoffart, L. M.; Stone, K. L.; Krebs, C.; Green, M. T. *J. Am. Chem. Soc.* **2006**, *128*, 11471−11474. (c) Dey, A.; Jiang, Y.; Ortiz de Montellano, P.; Hodgson, K. O.; Hedman, B.; Solomon, E. I. *J. Am. Chem. Soc.* **2009**, *131*, 7869−7878.

(32) Prokop, K. A.; de Visser, S. P.; Goldberg, D. P. *Angew. Chem., Int. Ed.* **2010**, *49*, 5091−5095.

(33) (a) Sastri, C. V.; Lee, J.; Oh, K.; Lee, Y. J.; Lee, J.; Jackson, T. A.; Ray, K.; Hirao, H.; Shin, W.; Halfen, J. A.; Kim, J.; Que, L.; Shaik, S.; Nam, W. *Proc. Nat. Acad. Sci. U. S. A.* **2007**, *104*, 19181−19186.

(b) Hirao, H.; Que, L.; Nam, W.; Shaik, S. *Chem.—Eur. J.* **2008**, *14*, 1740−1756.

(34) Tolman, C. A. *Chem. Rev.* **1977**, *77*, 313−348.

(35) Guzei, I. A.; Wendt, M. *Dalton Trans.* **2006**, 3991−3999.

(36) The halide and amide complexes show a larger difference in G parameter between $L^{Me,Ph3}$ and $L^{Me,iPr2}$ (the former being larger by ∼7%) than the imide complexes. See Supporting Information for details.

(37) The relative orientation of the binding pocket is the same in $L^{Me,iPr2}$FeNAd and **5**: the Fe=N−C plane is 53° (for $L^{Me,iPr2}$FeNAd) and 56° (for $L^{Me,Ph3}$FeNAd) out of the plane defined by the diketiminate backbone, suggesting that there is no change in orbital overlap for HAT and the effect on rate is dominantly steric.

(38) Al-Benna, S.; Sarsfield, M. J.; Thornton-Pett, M.; Ormsby, D. L.; Maddox, P. J.; Brès, P.; Bochmann, M. *J. Chem. Soc., Dalton Trans.* **2000**, 4247−4257.

(39) (a) Evans, D. F. *J. Chem. Soc.* **1959**, 2003−2005. (b) Schubert, E. M. *J. Chem. Educ.* **1992**, *69*, 62.

(40) Bolliger, J. L.; Frech, C. M. *Adv. Synth. Catal.* **2010**, *352*, 1075−1080.

(41) (a) Ammann, C.; Meier, P.; Merbach, A. E. *J. Magn. Reson.* **1982**, *46*, 319−321. (b) Kaplan, M. L.; Bovey, F. A.; Cheng, H. N. *Anal. Chem.* **1975**, *47*, 1703−1705.

(42) *APEX2*, V2.2-0; Bruker Analytical X-ray Systems: Madison, WI, 2007.

(43) *SADABS*, V2.10; Blessing, R. *Acta Crystallogr.* **1995**, *A51*, 33-38.

(44) Altomare, A.; Burla, M. C.; Camalli, M.; Cascarano, G. L.; Giacovazzo, C.; Guagliardi, A.; Moliterni, A. G. G.; Polidori, G.; Spagna, R. *SIR97: A new program for solving and refining crystal structures*; Istituto di Cristallografia, CNR: Bari, Italy, 1999.

(45) Sheldrick, G. M. *Acta Crystallogr.* **2008**, *A64*, 112−122.

(46) Spek, A. L. *PLATON: A multipurpose crystallographic tool*, version 300106; Utrecht University: Utrecht, The Netherlands, 2006.